




Adaptive backstepping controller design of quadrotor biplane for payload delivery

Nihal Dalwadi¹  | Dipankar Deb¹  | S. M. Muyeen² 

¹ Department of Electrical Engineering, Institute of Infrastructure Technology, Research and Management, Ahmedabad, India

² Department of Electrical Engineering, Qatar University, Doha, Qatar

Correspondence

S. M. Muyeen, Department of Electrical Engineering, Qatar University, Doha 2713, Qatar.
Email: sm.muyeen@qu.edu.qa

Abstract

Performance of the UAVs for a particular application can be enhanced by hybrid design, where take-off, hover, and landing happen like rotary-wing UAVs, and flies like fixed-wing UAVs. A backstepping controller and an adaptive backstepping controller are designed for trajectory tracking and payload delivery in a medical emergency or medical substance delivery like vaccine delivery in the presence of wind gust. Simulation results show that the backstepping controller effectively tracks the trajectory during the entire flight envelope, including take-off, hovering, the transition phase, level flight mode, and landing. A comparison between Backstepping, Integral Terminal Sliding Mode (ITSMC) and Adaptive Backstepping controllers for payload delivery show that the adaptive backstepping controller effectively tracks the altitude and attitude. ITSMC is capable of tracking the desired trajectory for a change in the mass but has sluggish response. The backstepping controller generates a steady-state error in altitude during the mass change in biplane quadrotor.

1 | INTRODUCTION

Nowadays, unmanned aerial vehicles (UAVs) find usage in the agriculture sector, surveillance, defense, mapping, disaster management etc. Most UAV designs are either fixed-wing or rotary-wing, but a hybrid design can enhance effectiveness and efficiency for some applications. A biplane quadrotor takes off, hovers, lands like rotary-wing UAVs, and flies at higher speeds like fixed-wing UAVs. Many researchers came up with different configurations and development methodologies of quadrotor biplanes. Hrishikeshavan et al. present a step-by-step development of biplane quadrotor for enhanced performance and experimentally examined a few essential design parameters such as wing aspect ratio, aerofoil profile, wing spacing, and offset between propeller axis and wing chord [1]. Sridharan et al. [2], propose a methodology for size and estimate the weight of primary load-carrying members as demonstrated on biplane tailsitter. Dawkins et al. propose a mathematical model and a PID controller for efficiency analysis of a micro quadrotor drone with airfoils and trim analysis suitable for nominal flight conditions [3]. Such algorithms iteratively learn a transition maneuver via flight trials using pitch angle and thrust regulation as per suitable control laws. Finally, Hrishikeshavan

et al. present the development of a linear quaternion-based control of a biplane quadrotor that transitions from hovering mode to level-flight mode [4].

UAVs have to perform optimized maneuvers in an environment with obstacles of different sizes and arbitrary motions. Mathew et al. address task scheduling and path planning problems for a team of cooperating vehicles performing autonomous deliveries in urban environments [5]. Elsewhere, Liu et al. present a formation control for a cluster of tail-sitters in transition between forward and vertical flight [6]. However, a robust nonlinear control method achieves trajectory tracking control in flight mode transitions in which the coordinate system and the controller structures (or the system parameters) do not need to switch [7]. The main objective of aerial robot control design is to guarantee safe operation and damage avoidance for the environment. Wagter et al. apply a Linear-Quadratic Regulator (LQR) controller on the tip-path plane model which is validated on an unstable Delfa Copter [8]. Mofid et al. address a sensor failure scenario in UAVs by considering a PID-SMC (Sliding mode control) technique when the upper bound of disturbance is known, and an adaptive PID-SMC maintains desired position when the disturbance bound is unknown [9]. Muthusamy et al. propose a novel bidirectional fuzzy brain emotional learning

This is an open access article under the terms of the [Creative Commons Attribution](https://creativecommons.org/licenses/by/4.0/) License, which permits use, distribution and reproduction in any medium, provided the original work is properly cited.

© 2022 The Authors. *IET Intelligent Transport Systems* published by John Wiley & Sons Ltd on behalf of The Institution of Engineering and Technology

controller for a quadcopter's trajectory tracking while handling payload uncertainties in real-time [10]. Backstepping method helps control longitudinal and lateral-directional motions for miniature UAV autopilots for desirable controller performance despite model parametric uncertainties or disturbances [11].

Observers estimate states that are not directly measurable for improved closed-loop stability. Chen et al. present a mathematical model of a quadrotor and using a combination of sliding mode control and backstepping control for position trajectory tracking with an adaptive observer-based fault estimation scheme [12]. Luo et al. analyze attitude and position control challenges for UAVs with a package linked by a wire and a robust neural network-based backstepping sliding mode control for observing the UAV flight path and chosen attitude with a suspended cable attached [13]. Dalwadi et al. [14] propose a nonlinear observer-based backstepping controller for trajectory tracking of tail-sitter UAV in the presence of wind gusts and periodic disturbances. A new control strategy [15] combines the backstepping and the dynamic inversion control methods to control the roll and yaw angle, altitude, and speed of fixed-wing UAVs and disturbance observer to estimate wind gusts. To control a two-link rigid-flexible wing, boundary control method designed on the working principle of bionics is used and validated through simulations [16]. Trajectory tracking problem of flapping-wing micro aerial vehicles in the longitudinal plane [17] based on kinematics, dynamics, aerodynamics forces, and torque use an adaptive control strategy under the hierarchical framework for autonomous tracking.

Intelligent controllers adjust themselves in a finite time with uncertain parameters, enabling the stabilization of aerial robots. A neural network-based adaptive controller is effective in a nonlinear ship-mounted crane system with inaccurate gravity compensation, ship roll motions, residual payload swing etc. [18–20]. Solution for the control problem in a class of multi-input multi-output (MIMO) underactuated systems subject to plant uncertainties and actuator dead-zones is provided [21]. Adaptive neural-network command-filtered tracking control structure of nonlinear systems with numerous actuator constrictions proposed in [22]. Lei et al. present robust adaptive tracking control of quadrotor in which control laws for the actuator inputs don't need motor speed to reduce a significant overshoot [23]. Dydek et al. apply direct and indirect model reference adaptive control to a lightweight, low-cost quadrotor for trajectory tracking and flight safety [24]. Zuo et al. address the trajectory tracking of UAVs in the presence of modeling uncertainties and external disturbances with L1 adaptive backstepping control [25].

Mofid et al. [26] propose an adaptive integral-type terminal sliding mode method for finite-time attitude and position tracking of a quadrotor UAV with model uncertainties and external disturbances. Adaptive super-twisting terminal sliding mode control introduced for quadrotor UAVs in the case of an unknown upper bound of the model uncertainty and wind disturbance gets validated by both simulation, and experiments [27]. Mofid et al. [28] propose an adaptive backstepping global sliding mode control technique of finite-time tracking control for attitude and position of the quadrotors in the presence of wind perturbation, input saturation, and model uncertainties in

quadrotor UAVs. Kourani et al. [29] establish an appropriate similarity between an adaptive backstepping control law and a standard PID controller for a class of second-order systems. Dhaybi et al. [30] propose a precise real-time estimation of the changeable mass and inertia tensor elements of a quadrotor carrying a variable payload based on a recursive least squares algorithm. Navabi et al. [31] propose an optimal adaptive sliding mode controller improved by particle swarm optimization (PSO) algorithm for the trajectory tracking of a quadcopter with model parameter uncertainties.

Hsu et al. presented a wavelet adaptive backstepping control system for a class of second-order nonlinear systems and applied it to a chaotic system [32]. Sun et al. proposed an adaptive backstepping control approach for active vehicle suspensions for improved ride comfort in the presence of parameter uncertainties [33]. Liu et al. proposed an adaptive control approach for tail sitter UAVs which does not need to switch the coordinate system or the controller structure and the parameters in different modes [34]. Wang et al. [35] is examined the difficulty of fuzzy-based adaptive event-triggered tracking control for a class of non-strict feedback systems within a fixed-time interval and presented a control structure that removes any possible singularity problem in the design process and guarantees closed-loop signal boundedness.

Payloads combined with UAVs use a mechanical arrangement of cables. Many researchers have designed different adaptive or observer based controllers to compensate or adapt for the mass variation or stabilize the swinging payload with cable. Oshman et al. propose a method of utilizing the outputs of rate gyros and other available data of mounted sensors for autonomous attitude estimation of a UAV carrying an inertially stabilized payload [36]. Qian et al. develop a path following controller based on uncertainty and disturbance estimator for a quadrotor with a cable-suspended payload [37]. In contrast, Yang et al. use a nonlinear controller to maintain a quadrotor's desired position while carrying a suspended payload [38]. Lee et al. propose a novel trajectory generation to minimize the swing motion and an effective anti-sway tracking control technique based on Linear quadratic (LQ) control for a quadrotor UAV with a cable-suspended payload [39]. A novel online anti-swing trajectory planning proposed for a quadrotor slung load system contains two parts: a target positioning and anti-swing [40]. Outeiro et al. present a method for height and yaw angle control of a quadrotor transporting an unknown load [41]. Qian et al. [42] present a novel guidance and control design for a parcel tied to a drone to allow for a soft landing and ensure swing-free payload transportation.

The quadrotor biplane has a variable pitch or fixed pitch H-shaped quadrotor with two fixed wings attached to the parallel limbs. Advantages of variable pitch propellers are (i) greater control authority and control bandwidth, (ii) improved maneuverability and gust rejection capability, (iii) hovering (3200 rpm), and level flight (2000 rpm) modes have different rpm, ensuring reduced power consumption. In addition, the biplane quadrotor has good stability and long flight endurance, encouraging usage for transport of medical substances like blood, first aid kit, corona vaccine etc., food packet in flood-type scenarios, and

small ammunition in the war against terror. The key advantages of use over a helicopter are that it is a cost-effective solution when we need lightweight packet drops in multiple areas, performs an autonomous flight, and comes in a compact structure. Furthermore, compared to conventional UAVs, Quadrotor Biplane provides long flight, and internal combustion (IC) engine or Li-ion battery is usable for the power plant, eliminating the need for battery recharge.

Phillips et al. present a quadrotor biplane design and testing in hover flight mode for remotely operated aerial package delivery capability involving a solenoid mechanism to ensure that the payload door stays locked with the drone in transition flight mode [43]. Phillips et al. [44] experimentally validate the design of quadrotor biplane using a Quaternion feedback control law and package delivery functionality for both quadrotor and fixed-wing mode with 3.76 kg gross take-off weight and 0.45 kg payload. Chipade et al. present a theoretical design and proof of concept flight demonstration of a novel variable-pitch quadrotor biplane for payload delivery up to 6 kg as applied on open-source autopilot for hovering state, delivery range of 32 km, the level flight speed of 20 m/s, and a cruising height of 500 m above the sea [45]. Fixed pitch propeller-based design of hybrid UAVs is easy but provides poor stability and control authority. While Swarnkar et al. present a 6-DOF (degree of freedom) flight dynamics model and dynamic inversion based nonlinear controller for all modes of biplane quadrotor [46]. Govindarajan et al. present a conceptual sizing and performance valuation of four VTOL configurations to conclude that wing-borne designs like the quadrotor biplane and tricopter are capable of quickly delivering packages [47]. In this paper, we designed backstepping controller for trajectory tracking and an adaptive backstepping controller for a scenario where we drop 6 kg weight at location a , and pick up 3 kg weight each from locations b and c , while reducing altitude by only 2 m, and maintaining 20 m height to get back to the original location. Furthermore, the controller facilitates stable flight and trajectory following, aided by adaptive laws that help hold altitude during a change in the total biplane mass, and performs better than the Integral Terminal Sliding mode control (ITSMC). We propose

- A backstepping controller for the trajectory tracking of the entire flight envelope effectively controls in all three modes: (i) Quadrotor mode, (ii) Transition mode, and (iii) Fixed-wing mode.
- An adaptive backstepping control strategy handles the mass change during the delivery and pick up of payloads like vaccines.
- A simulation study by applying wind gust disturbance during payload delivery to compare the adaptive backstepping control strategy with the ITSMC and backstepping control methods.

Initially, the total weight of the biplane quadrotor (with packets of net weight 6 kg) is 18 kg. As shown in Figure 1, in the first phase, take-off happens while holding the $x - y$ position. After reaching the desired altitude in the second phase, the transition maneuver happens and converts the vehicle to a fixed-wing

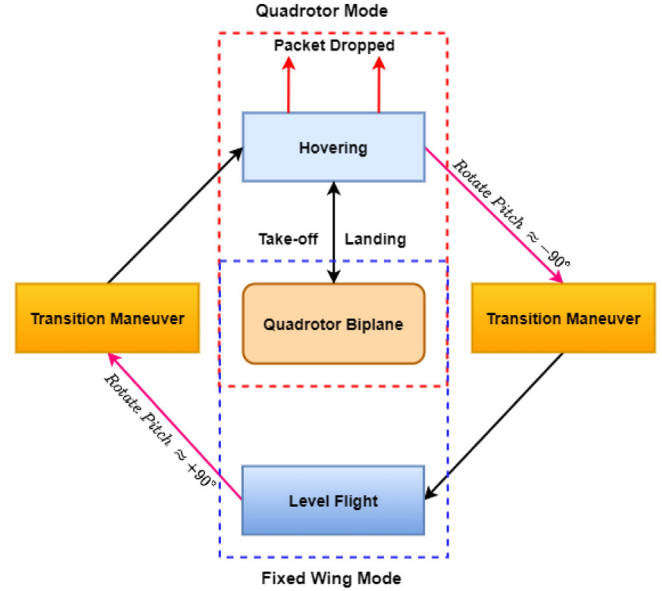


FIGURE 1 Quadrotor biplane

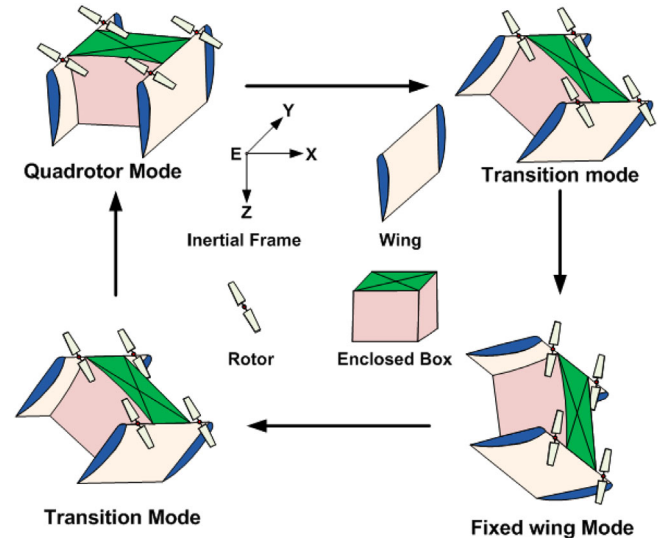


FIGURE 2 Quadrotor biplane animated picture

aircraft travelling up to 1022 m at 15 m/s, to again perform transition maneuver.

Figure 2 shows an animated picture of the quadrotor biplane for better visualization of transition between the quadrotor and fixed-wing mode vis-a-vis. The enclosed box contains a battery, embedded system, and payload. While hovering at 20 m altitude, when commanded to drop 6 kg weight, the biplane performs transition maneuver and flies like a fixed-wing UAV. Then, it again reduces the altitude from 20 m to 2 m and picks up 3kg payload two times from two different locations. Then, under the presence of wind gusts, the biplane gets back to its origin and lands.

The rest of this paper is organized as follows: Section 2 presents the biplane quadrotor dynamics. In Section 3, we design a backstepping controller for trajectory tracking, and in

Section 4, we develop an adaptive backstepping controller for packet delivery and trajectory tracking, combining takeoff, hovering, transition, level flight mode, and landing phases, followed by control allocation in Section 5. Finally, simulation results demonstrate the efficacy of the adaptive backstepping controller over with ITSMC in Section 6.

2 | MATHEMATICAL MODEL OF BIPLANE DRONE

Biplane quadrotor can be powered by a small IC engine [45], or conventional lithium polymer or lithium iron battery [43]. We consider quadrotor biplane with IC engine as the power plant of 12 kg weight. The mathematical model considers the body frame because most flight phases are in the quadrotor frame. Gravitational force, aerodynamics forces are resolved along with the body axis. Likewise, the total moment is due to the propulsive and aerodynamic forces. Biplane dynamics are

$$\begin{bmatrix} \ddot{x} \\ \ddot{y} \\ \ddot{z} \end{bmatrix} = \frac{1}{m} \begin{bmatrix} F_{ax} \\ F_{ay} \\ -T + F_{az} \end{bmatrix} + g \begin{bmatrix} -s\theta \\ c\theta s\phi \\ c\theta c\phi \end{bmatrix} + \begin{bmatrix} rv - qw \\ pw - ru \\ qu - pv \end{bmatrix}, \quad (1)$$

$$\begin{bmatrix} \ddot{\phi} \\ \ddot{\theta} \\ \ddot{\psi} \end{bmatrix} = \begin{bmatrix} (b_1 r + b_2 p)q + b_3(L_a + L_t) + b_4(N_a + N_t) \\ b_5 pr - b_6(p^2 - r^2) + b_7(M_a + M_t) \\ (b_8 p - b_2 r)q + b_4(L_a + L_t) + b_9(N_a + N_t) \end{bmatrix}, \quad (2)$$

where u, v and w are the linear velocity components, p, q and r are angular velocity components, L_t, M_t , and N_t are roll, pitch, and yaw moments, L_a, M_a , and N_a are the roll, pitch and yaw moments due to aerodynamics forces acting on the biplane quadrotor such that

$$\begin{bmatrix} F_{ax} \\ F_{ay} \\ F_{az} \end{bmatrix} = \begin{bmatrix} s\alpha c\alpha & -s\alpha s\beta & c\alpha \\ s\beta & c\beta & 0 \\ -c\alpha c\beta & c\alpha s\beta & s\alpha \end{bmatrix} \begin{bmatrix} -D \\ Y \\ -L \end{bmatrix}, \quad (3)$$

where α is the angle of attack, β is the side slip angle, D, Y and L are the aerodynamic forces acting on roll, pitch and yaw axis of quadrotor biplane. The moments and aerodynamic forces are defined subsequently. Inertial terms are defined as constants b_i :

$$\begin{bmatrix} b_1 \\ b_2 \\ b_3 \\ b_4 \\ b_8 \\ b_9 \end{bmatrix} = \frac{1}{I_x I_x - I_{xz}^2} \begin{bmatrix} (I_y - I_x)I_x - I_{xz}^2 \\ (I_x - I_y + I_x)I_{xz} \\ I_x \\ I_{xz} \\ (I_x - I_y)I_x + I_{xz}^2 \\ I_x \end{bmatrix},$$

$$\begin{bmatrix} b_5 \\ b_6 \\ b_7 \end{bmatrix} = \frac{1}{I_y} \begin{bmatrix} (I_x - I_x) \\ I_{xz} \\ 1 \end{bmatrix}. \quad (4)$$

The vehicle speed (V) and active pressure (Q_∞) acting on it are

$$V = \sqrt{u^2 + v^2 + w^2}, \quad Q_\infty = \frac{1}{2}\rho V^2, \quad (5)$$

where ρ is the air density (kg/m^3). Quadrotor frame is aligned with the inertial frame with center of gravity of the biplane quadrotor and the rotational matrix is given as

$$\begin{bmatrix} \dot{x} \\ \dot{y} \\ \dot{z} \end{bmatrix} = \begin{bmatrix} c\phi c\psi & s\phi s\theta c\psi - c\phi s\psi & c\phi s\theta c\psi + s\phi s\psi \\ c\theta s\psi & s\phi s\theta s\psi + c\phi c\psi & c\phi s\theta s\psi - s\phi c\psi \\ -s\theta & s\phi c\theta & c\phi c\theta \end{bmatrix} \begin{bmatrix} u \\ v \\ w \end{bmatrix}, \quad (6)$$

where $c(\cdot) = \cos(\cdot)$ and $s(\cdot) = \sin(\cdot)$. The moments due to aerodynamic forces are defined as

$$\begin{bmatrix} L_a \\ M_a \\ N_a \end{bmatrix} = \begin{bmatrix} 0.5\rho V^2 S b C_{l_c} \\ 0.5\rho \bar{c} V^2 S C_{m_c} \\ 0.5\rho V^2 S b C_{n_c} \end{bmatrix}, \quad (7)$$

where C_{l_c}, C_{m_c} and C_{n_c} are the roll, pitch and yaw moments coefficients, S is wing area (m^2), b is wing span (m), c is chord of the rotor blade, \bar{c} is the mean aerodynamics chord (m), and

$$C_{l_c} = C_{l_\beta}\beta + C_{l_p}\frac{p_w b}{2V} + C_{l_r}\frac{r_w b}{2V} \quad (8)$$

$$C_{n_c} = C_{n_\beta}\beta + C_{n_p}\frac{p_w b}{2V} + C_{n_r}\frac{r_w b}{2V}, \quad (9)$$

such that $C_{l_\beta}, C_{l_p}, C_{l_r}, C_{n_\beta}, C_{n_p}$ and C_{n_r} values are provided [46] after studying physical representation of the system. Subscript w is for wing body axis.

For the simulation, a NACA 0012 aerofoil with XFOIL code helps predict the aerodynamic performance at Reynolds number 0.25×10^6 . XFOIL is easy to use as compared to more complex CFD analysis software like ANSYS Fluent and OpenFoam at low speed, and single element aerofoils [48]. XFOIL is also relatively fast and accurate compared to complex CFD analysis software [49]. After getting the lift, drag, and pitch moment coefficient values from XFOIL polynomial functions, we used the polyfit function in MATLAB to generate the polynomial functions of aerodynamics coefficients lift (C_l), drag (C_d) and pitch moment (C_{m_c}) versus angle of attack (α) and coefficients Vs. α graph is given in Figure 3.

3 | CONTROLLER DESIGN

Next, we discuss backstepping controller design for all three modes.

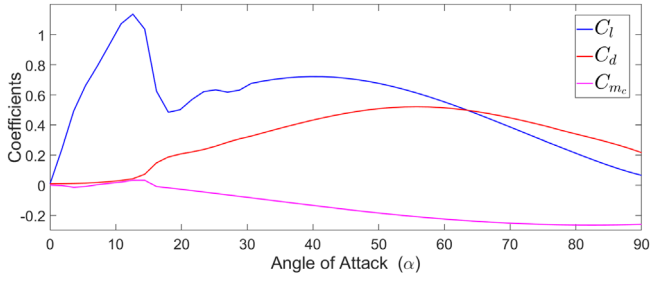


FIGURE 3 C_l , C_d and C_{m_c} versus angle of attack (AoA)

3.1 | Quadrotor mode

No substantial aerodynamic forces are acting, and the wings of this drone produce the moments during takeoff, hovering, the initial transition phase, and the landing phase. It can thus be seen as a simple quadrotor drone with $[F_{ax} F_{ay} F_{az}] = [0 \ 0 \ 0]$ and aerodynamic moments $[L_d M_d N_d] = [0 \ 0 \ 0]$. The motion equation defined helps derive the controller in the quadrotor frame. In quadrotor mode consisting of a hovering flight phase, only thrust and gravitational forces are acting on it. In general, the drone propulsion system generates 1.5 to 2 times higher lift than its net weight. Usage of Newton's second law of motion determines the translation dynamics in the inertial frame given as

$$m \begin{bmatrix} \ddot{x} \\ \ddot{y} \\ \ddot{z} \end{bmatrix} = \begin{bmatrix} 0 \\ 0 \\ mg \end{bmatrix} + R \begin{bmatrix} 0 \\ 0 \\ -T \end{bmatrix}, \quad (10)$$

$$R = \begin{bmatrix} c\phi c\psi & s\phi s\theta c\psi - c\phi s\psi & c\phi s\theta c\psi + s\phi s\psi \\ c\theta s\psi & s\phi s\theta s\psi + c\phi c\psi & c\phi s\theta s\psi - s\phi c\psi \\ -s\theta & s\phi c\theta & c\phi c\theta \end{bmatrix}. \quad (11)$$

It is seen in Figure 4 that the desired trajectory $[x_d \ y_d \ z_d]$ and yaw angle $[\psi_d]$ given to the position and attitude controller. Position controller generates desired thrust $[T]$ to track the desired altitude and also generates desired roll and pitch angle. Using these desired roll, pitch, and yaw angles, the attitude controller generates roll, pitch, and yaw moments $[L_t \ M_t \ N_t]$. Section 5 explains the associated control allocation.

The trajectory tracking of the biplane quadrotor is designed based on a recursive use of Lyapunov functions on a nonlinear technique called backstepping control. The main idea is to recursively choose appropriate state variables as virtual inputs for lower dimension subsystems, while the Lyapunov functions intended for each stable virtual controller ensure that the control law guarantees system stability [50]. We first demonstrate the backstepping controller design for attitude control, and by using the same procedure, design the position controller. Using (2), with zero aerodynamic moments, the error between the actual and the desired roll angle is

$$e_\phi = \phi - \phi_d. \quad (12)$$

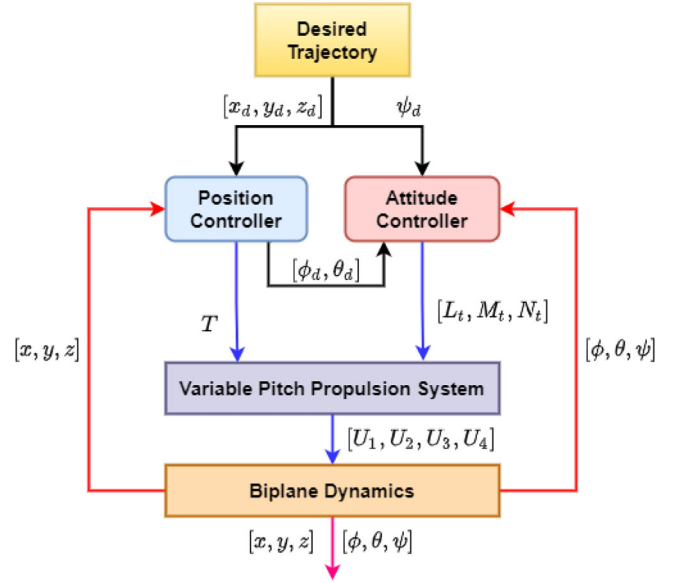


FIGURE 4 Quadrotor mode controller design

A positive definite function is defined $V_{QM_\phi} = \frac{1}{2}e_\phi^2$ and its time derivative is $\dot{V}_{QM_\phi} = e_\phi \dot{e}_\phi = e_\phi \dot{e}_p - k_\phi e_\phi^2$, $k_\phi > 0$. where $e_p = p - p_d$. To satisfy this condition a virtual control $p_d = \dot{\phi}_d - k_\phi e_\phi$ is chosen such that

$$e_p = p - p_d = p - \dot{\phi}_d + k_\phi e_\phi. \quad (13)$$

The next step is to enhance V_{QM_ϕ} with quadratic term in e_p , To get positive definite function as $V_{QM_p} = \frac{1}{2}e_p^2 + V_{QM_\phi}$, and time derivative is

$$\begin{aligned} \dot{V}_{QM_p} &= e_p((b_1 r + b_2 p)q + b_3 L_t + b_4 N_t - \ddot{\phi}_d + k_\phi \dot{e}_\phi) \\ &\quad - k_\phi e_\phi^2 + e_\phi \dot{e}_p. \end{aligned} \quad (14)$$

By equation (14) control law for a roll subsystem can be define as

$$L_t = \frac{1}{b_3}(-e_\phi - k_p e_p + \ddot{\phi}_d - k_\phi \dot{e}_\phi - (b_1 r - b_2 p)q - b_4 N_t). \quad (15)$$

so that $\dot{V}_{QM_p} = -k_\phi e_\phi^2 - k_p e_p^2$ which guarantees asymptotic stable system for appropriately chosen $k_\phi, k_p > 0$.

As explained earlier, by using same calculation procedure we can define control law for pitch and yaw angle as well as position

$$M_t = \frac{1}{b_7}(\ddot{\theta}_d - e_\theta - k_q e_q - k_\theta \dot{e}_\theta + b_6(p^2 - r^2) - b_5 p r), \quad (16)$$

$$N_t = \frac{1}{b_9} (\ddot{\psi}_d - e_\psi - \kappa_r e_r - \kappa_\psi \dot{e}_\psi - (b_8 p - b_2 r)q - b_4 L_t), \quad (17)$$

$$T = \frac{m}{c\phi c\theta} (e_x + e_w \kappa_w - \ddot{x}_d + \kappa_x \dot{e}_x + g), \quad (18)$$

$$u_x = \frac{m}{T} (e_x + \kappa_u e_u - \ddot{x}_d + \kappa_x \dot{e}_x), \quad (19)$$

$$u_y = \frac{m}{T} (e_y + \kappa_v e_v - \ddot{y}_d + \kappa_y \dot{e}_y). \quad (20)$$

By using (15) and (17), the control law for the roll subsystem is

$$L_t = \left(\frac{b_9}{b_3 b_9 - b_4} \right) (-e_\phi - \kappa_p e_p - \kappa_\phi \dot{e}_\phi + \ddot{\phi}_d - b_1 r q - b_2 p q - \frac{b_4}{b_9} (-e_\psi - \kappa_r e_r - \kappa_\psi \dot{e}_\psi + \ddot{\psi}_d - b_8 p q + b_2 q r)). \quad (21)$$

Using (19) and (20), the desired roll and pitch angle are calculated as

$$\begin{aligned} \phi_d &= \arcsin \left(\frac{u_x - u_y}{s\psi + c\psi} \right), \\ \theta_d &= \arcsin \left(\frac{u_x - u_y - s\phi(s\psi - c\psi)}{2c\phi c\psi} \right). \end{aligned} \quad (22)$$

3.2 | Transition mode

The aim of a transition controller is to allow the drone to traverse move from quadrotor mode to level flight mode and vice versa. Biplane quadrotor drone achieves level flight where lift force supports most of the weight caused by the double wing. In quadrotor mode, pitch angle (θ) $\approx 0^\circ$ to flight mode where the pitch angle is (θ) $\approx 90^\circ$, is achieved to rotate the biplane about pitch angle to $\approx 90^\circ$. When the pitch angle of the biplane starts decreasing from 0° , the perpendicular component of thrust generated by the rotors start reducing, and the two wings primarily generate no substantial lift force till it transitions past the stall angle of attack.

The desired pitch angle transition contains two phases: (a) primary transition phase and (b) ending transition phase. In the primary phase, the commanded pitch angle reduces linearly from $\theta_{Q_{hover}}$ (hover pitch attitude) to an internal pitch angle, $\theta_{Q_{sw}}$ governed by the angle of attack (AoA) and desired flight path angle (γ) [51]. This transition phase is activated only for a 1 s duration from fixed-wing to quadrotor mode to accomplish vertical landing. The pitch angle increases from θ_{fl} to θ_{vt} to achieve vertical landing at the desired velocity. In the transition mode, we have no control over the $x - y$ position of the biplane; only attitude and altitude get controlled. In the transition mode,

control laws are the same as defined in the quadrotor mode, but the aerodynamic forces are significant.

Using (2), the error generated in the roll angle is defined as, $e_\phi = \phi - \phi_d$. A positive definite function is defined based on the error is $V_{TM_\phi} = \frac{1}{2} e_\phi^2$ and by tacking it's time derivative we get $\dot{V}_{TM_\phi} = e_\phi \dot{e}_\phi - \delta_\phi e_\phi^2$, $\delta_\phi > 0$. where $e_p = p - p_d$.

To satisfy this condition a virtual control $p_d = \dot{\phi}_d - \delta_\phi e_\phi$ is chosen such that

$$e_p = p - p_d = p - \dot{\phi}_d + \kappa_\phi e_\phi. \quad (23)$$

Now, to enhance V_{TM_ϕ} with quadratic term in e_p , To get positive function as $V_{TM_p} = \frac{1}{2} e_p^2 + V_{TM_\phi}$ and time derivative is

$$\begin{aligned} \dot{V}_{TM_p} &= e_p ((b_1 r + b_2 p)q + b_3(L_t + L_a) + b_4(N_t + N_a) \\ &\quad - \ddot{\phi}_d + \kappa_\phi \dot{e}_\phi) - \delta_\phi e_\phi^2 + e_\phi \dot{e}_p. \end{aligned} \quad (24)$$

By using (24), the control law for the transition mode is designed as

$$\begin{aligned} L_t &= \left(\frac{b_9}{b_3 b_9 - b_4} \right) (-e_\phi - \kappa_p e_p - \kappa_\phi \dot{e}_\phi + \ddot{\phi}_d - b_1 r q - b_2 p q \\ &\quad - \frac{b_4}{b_9} (-e_\psi - \kappa_r e_r - \kappa_\psi \dot{e}_\psi + \ddot{\psi}_d - b_8 p q + b_2 q r)) - L_a, \end{aligned} \quad (25)$$

so that $V_{TM_p} = -\kappa_1^2 e_\phi^2 - \kappa_2^2 e_p^2 \leq 0$, and using similar steps, the control law for the pitch, yaw and altitude subsystems are

$$\begin{aligned} M_t &= \frac{1}{b_7} (\ddot{\theta}_d - e_\theta - \kappa_q e_q - \kappa_\theta \dot{e}_\theta + b_6(p^2 - r^2)) \\ &\quad - M_a - \frac{b_5}{b_7} p r, \end{aligned} \quad (26)$$

$$\begin{aligned} N_t &= \frac{1}{b_9} (-e_\psi - \kappa_r e_r + \ddot{\psi}_d - \kappa_\psi \dot{e}_\psi - (b_8 p - b_2 r)q \\ &\quad - b_4(L_t + L_a) - b_9 N_a), \end{aligned} \quad (27)$$

$$T = \frac{m}{c\phi c\theta} \left(e_x + e_w \kappa_w - \ddot{x}_d + \kappa_x \dot{e}_x + g - \frac{F_{ax}}{m} \right). \quad (28)$$

3.3 | Level flight mode

In this mode, the dynamics are similar to conventional fixed-wing aircraft or helicopters [52, 53]. Biplane dynamics (1) and (2), where variables are defined with respect to the body frame. We need to transform these equations with respect to fixed wing

axis and that can be done by

$$\begin{bmatrix} v_x \\ v_y \\ v_z \end{bmatrix}_W = \begin{bmatrix} 0 & 0 & -1 \\ 0 & 1 & 0 \\ 1 & 0 & 0 \end{bmatrix} \begin{bmatrix} v_x \\ v_y \\ v_z \end{bmatrix}_Q. \quad (29)$$

Inertial matrix, body transitional velocities and body angular rates in a fixed wing frame can be defined using

$$\begin{bmatrix} u & v & w \end{bmatrix}_W^T = \begin{bmatrix} -w & v & u \end{bmatrix}_Q^T, \quad \begin{bmatrix} p & q & r \end{bmatrix}_W^T = \begin{bmatrix} -r & q & p \end{bmatrix}_Q^T. \quad (30)$$

By using these equations, biplane quadrotor fixed wing mode dynamics are

$$\dot{x} = c\theta c\psi u + (s\phi s\theta c\psi - c\phi s\psi)v + (c\phi s\theta c\psi + s\phi s\psi)w, \quad (31)$$

$$j = c\theta s\psi u + (s\phi s\theta s\psi + c\phi c\psi)v + (c\phi s\theta s\psi - s\phi c\psi)w, \quad (32)$$

$$\dot{\xi} = -u s\theta + v s\phi c\theta + w c\phi c\theta, \quad (33)$$

$$\dot{u} = \frac{F_{ax}}{m} - g s\theta + pv - qu + \frac{T}{m}, \quad (34)$$

$$\dot{v} = \frac{F_{ay}}{m} + g c\theta s\phi + pw - ru, \quad (35)$$

$$\dot{w} = \frac{F_{az}}{m} + g c\theta c\phi + rv - qw, \quad (36)$$

$$\begin{aligned} \dot{p} = & -pq(b_{w3} + b_{w9}) - qr(b_{w11} - b_{w12}) - b_{w13}(L_a + L_t) \\ & + b_{w5}(N_a + N_t), \end{aligned} \quad (37)$$

$$\dot{q} = b_{w8}r^2 + b_{w9}p^2 + 2b_{w10}pr + b_{w7}(M_t + M_a), \quad (38)$$

$$\begin{aligned} \dot{r} = & pq(b_{w1} + b_{w2}) + qr(b_{w3} - b_{w4}) + b_{w5}(L_t + L_a) \\ & - b_{w6}(N_t + N_a), \end{aligned} \quad (39)$$

$$\dot{\phi} = p + q s\phi t\theta + r c\phi t\theta, \quad (40)$$

$$\dot{\theta} = q c\phi - r s\phi, \quad (41)$$

$$\dot{\psi} = q \frac{s\phi}{c\theta} + r \frac{c\phi}{c\theta}, \quad (42)$$

where $b_{w1} = I_{x\tilde{x}}(I_y + I_{x\tilde{x}})/B$, $b_{w2} = I_{\tilde{x}}^2/B$, $b_{w3} = I_{x\tilde{x}}(I_x + I_y)/B$, $b_{w4} = I_x I_y/B$, $b_{w5} = I_{x\tilde{x}}/B$, $b_{w6} = I_{\tilde{x}}/B$, $b_{w7} = 1/I_y$,

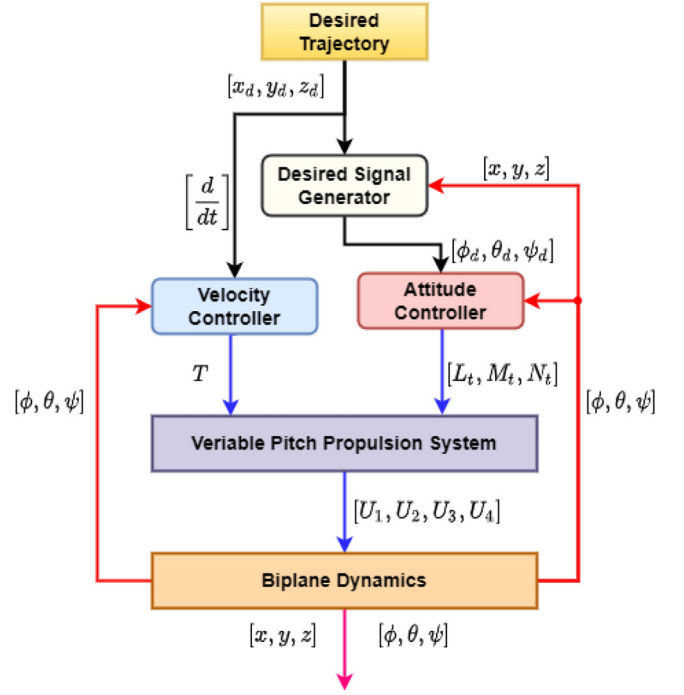


FIGURE 5 Fixed wing mode controller design

$b_{w8} = I_x/I_y$, $b_{w9} = I_{\tilde{x}}/I_y$, $b_{w10} = I_{x\tilde{x}}/I_y$, $b_{w11} = I_x^2/B$, $b_{w12} = I_{x\tilde{x}}(I_y - I_{x\tilde{x}})/B$, $b_{w13} = I_x/B$ and $B = I_x I_{\tilde{x}} - I_{x\tilde{x}}^2$.

Control laws for level flight mode are defined as shown in Figure 5. In the fixed-wing mode, input signals are $[x_d \ y_d \ z_d]$, and accordingly, calculation of the desired pitch and yaw angles take place. We consider roll angle as the function of the yaw angle, with $y - z$ position controlled by the pitch and yaw angle, and the x position controlled by the Thrust generated by the aerodynamic forces and the four rotors. The velocity controller generates the Thrust, and the attitude controller tracks the desired attitude of the biplane quadrotor and helps calculate the moments. Using (31), and the desired velocity for fixed-wing mode, the error in velocity is

$$e_x = x - x_d. \quad (43)$$

A positive definite function is defined as $V_{FM_x} = \frac{1}{2}e_x^2$ by tacking first time derivative and using equation (31), we get

$$\begin{aligned} \dot{V}_{FM_x} = & e_x (c\theta c\psi u_d + (s\phi s\theta c\psi - c\phi s\psi)v \\ & + (c\phi s\theta c\psi + s\phi s\psi)w - \dot{x}_d), \end{aligned} \quad (44)$$

so for desired u_d velocity, control law can be designed as

$$\begin{aligned} u_d = & \frac{-1}{c\theta c\psi} (k_x e_x + (s\phi s\theta c\psi + c\phi s\psi)v + (c\phi s\theta c\psi + s\phi s\psi)w \\ & + \dot{x}_d), \end{aligned}$$

so that $\dot{V}_{FM} = -k_x e_x^2$ which guarantees asymptotic stable system for appropriately chosen $k_x > 0$. Now using (45), we calculate the desired thrust. So the error in x direction velocity is defined as

$$e_u = u - u_d, \quad (45)$$

A positive definite function is define as $V_{FM_u} = \frac{1}{2} e_u^2$. Tracking time derivative and using (34), we get

$$\dot{V}_{FM_u} = e_u \left(\frac{F_{ax}}{m} - g \sin \theta + pv - qu + \frac{T}{m} - \dot{u}_d \right). \quad (46)$$

Control law for desired thrust can be defined as

$$T = m \left(k_u e_u - \frac{F_{ax}}{m} + g \sin \theta - pv + qu + \dot{u}_d \right), \quad (47)$$

so that $\dot{V}_{FM_u} = -k_u e_u^2$ which guarantees asymptotic stable system for appropriately chosen $k_u > 0$. Desired pitch and yaw angle can calculate [54] as

$$\theta_d = \sin^{-1} \left(\frac{\dot{z}_d - k_z (z_c - z_d)}{\sqrt{a^2 + b^2}} \right) + \tan^{-1} \left(\frac{u}{v \sin \phi + w \cos \phi} \right), \quad (48)$$

$$\psi_d = \tan^{-1} \left(\frac{\dot{y}_d - k_y (y_d - y)}{\dot{x}_d + k_x (x_d - x)} \right). \quad (49)$$

where z_d is desired altitude, x_d and y_d are desired x and y positions, k_x , k_y , k_ϕ and k_z are tunable gains. We consider roll angle as a linear function of yaw angle, given as

$$\phi_d = k_\phi (\psi - \psi_d). \quad (50)$$

As per the desired angle, control law for the roll, pitch and yaw moment are calculated. For the yaw subsystem, the error between desired and actual roll angle is given as

$$e_\phi = \phi - \phi_d. \quad (51)$$

A positive definite function is defined as $V_{FM_\phi} = \frac{1}{2} e_\phi^2$, taking time-derivative, and using (40), we get the desired roll angle rate as

$$\dot{V}_{FM_\phi} = e_\phi (p + q \sin \phi \dot{\theta} + r \cos \phi \dot{\theta} - \dot{\phi}_d). \quad (52)$$

So control law can be defined for the desired roll angle rate p_d as

$$p_d = (-k_\phi e_\phi - q \sin \phi \dot{\theta} - r \cos \phi \dot{\theta} + \dot{\phi}_d). \quad (53)$$

By using (37) and (53), error between roll angle rate is given by $e_p = p - p_d$. Considering $V_{FM_p} = \frac{1}{2} e_p^2$, we get

$$\begin{aligned} \dot{V}_{FM_p} = e_p &(-pq(b_{w3} + b_{w9}) - qr(b_{w11} - b_{w12}) \\ &- b_{w13}(L_a + L_t) + b_{w5}(N_a + N_t) - \dot{p}_d). \end{aligned} \quad (54)$$

The control law for the roll angle rate is defined as

$$\begin{aligned} L_t = \frac{1}{b_{w13}} &(k_p e_p - pq(b_{w3} + b_{w9}) + qr(b_{w12} - b_{w11}) \\ &+ b_{w5}(N_a + N_t) - \dot{p}_d), \end{aligned} \quad (55)$$

such that $\dot{V}_{FM_p} = -k_p e_p^2$ guarantees asymptotic stable system for appropriately chosen $k_p > 0$. Using same procedure, we define control law for the pitch and yaw subsystem:

$$q_d = \frac{1}{c\phi} (-k_\theta e_\theta - r \sin \phi + \dot{\theta}_d), \quad (56)$$

$$r_d = \frac{1}{c\theta \cos \phi} (k_\psi e_\psi - q \sin \phi \dot{\theta} + \dot{\psi}_d), \quad (57)$$

$$\begin{aligned} M_t = \frac{-1}{b_{w7}} &(k_q e_q + b_{w8} r^2 + b_{w9} p^2 + 2prb_{w10} \\ &+ b_{w7} M_a - \dot{q}_d), \end{aligned} \quad (58)$$

$$\begin{aligned} N_t = \frac{1}{b_{w6}} &(k_r e_r + pq(b_{w1} + b_{w2}) + qr(b_{w3} - b_{w4}) \\ &+ b_{w5}(L_t + L_a) - b_{w6} N_a - \dot{r}_d). \end{aligned} \quad (59)$$

Using (59), we rewrite (55) as

$$\begin{aligned} L_t = &\left(\frac{b_{w6}}{b_{w6} b_{w13} - b_{w5}^2} \right) (-pq(b_{w3} + b_{w4}) - qr(b_{w11} - b_{w12}) \\ &+ k_p e_p - \dot{p}_d + \left(\frac{b_{w5}}{b_{w6}} \right) (pq(b_{w1} + b_{w2}) + qr(b_{w3} + b_{w4}) \\ &+ k_r e_r - \dot{r}_d)) - L_a. \end{aligned} \quad (60)$$

4 | ADAPTIVE BACKSTEPPING CONTROLLER DESIGN

Biplane quadrotor can drop or pick up payload only in the hover state, and so when commanded to pick up or drop packets, it transitions from flight mode. Figure 6 shows a block diagram of adaptive backstepping control. When a mass change occurs, the controller gets updated by the adaptive law to hold the desired altitude and attitude. With an initial net weight of 18 kg, the Biplane drops 6 kg weight at 20 m height and then picks up two

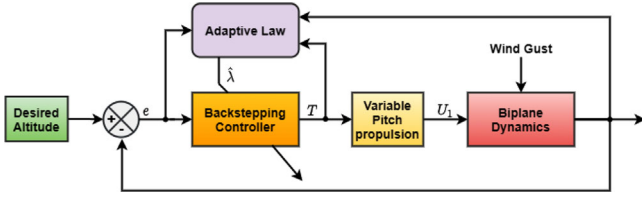


FIGURE 6 Adaptive backstepping control

packets of 3kg each at different locations of 2 m height, respectively.

We consider mass as an uncertain parameter and the adaptive law such that the controller adapts to change in mass in finite time. We consider the altitude subsystem because in quadrotor mode, the weight of the biplane is balanced by the thrust. By using (10) but for an uncertain mass m^* , the altitude subsystem is written as

$$\ddot{z} = g - T\lambda^* c\theta c\phi, \quad (61)$$

where $\lambda^* = \frac{1}{m^*}$. During the payload drop or pick, the biplane should hold the desired altitude. The error in altitude is given as

$$e_z = z - z_d. \quad (62)$$

A positive definite function is defined as $V_{QM_z} = \frac{1}{2}e_z^2$ and time derivative is $\dot{V}_{QM_z} = e_z\dot{e}_z = e_z e_w - \kappa_z e_z^2$, $\kappa_z > 0$ with $e_w = w - w_d$. To satisfy this condition, a virtual control $w_d = \dot{z}_d - \kappa_z e_z$ is chosen such that $e_w = w - \dot{z}_d + \kappa_z e_z$. The next step is to enhance V_{QM_z} with quadratic term in e_w is to have a positive definite $V_{QM_w} = \frac{1}{2}e_w^2 + V_{QM_z} + \frac{1}{2\gamma}\tilde{\lambda}^2$, where $\tilde{\lambda} = \lambda^* - \hat{\lambda}$ for an estimate $\hat{\lambda}$ and an adaptation gain $\gamma > 0$. By differentiating, we get

$$\begin{aligned} \dot{V}_{QM_w} = & -\kappa_z e_z^2 + e_w(-T(\tilde{\lambda} + \hat{\lambda})c\phi c\theta + g - \ddot{z}_d + \kappa_z \dot{e}_z) \\ & + e_z e_w - \frac{1}{\gamma}\tilde{\lambda}\dot{\tilde{\lambda}}. \end{aligned} \quad (63)$$

Observing (63), a choice of $\dot{\hat{\lambda}} = -\gamma e_w T c\phi c\theta$ leads to cancellation of terms. However, for robustness, considering the drone's physical lower bound of $\underline{\lambda} = \frac{1}{m}$, we design the adaptive update law as

$$\dot{\hat{\lambda}} = \begin{cases} -\gamma e_w T c\phi c\theta, & \text{if } |\hat{\lambda}(t)| > \underline{\lambda} \\ -\gamma e_w T c\phi c\theta, & \text{if } |\hat{\lambda}(t)| = \underline{\lambda} \ \& \ e_w T c\phi c\theta \operatorname{sgn}(\hat{\lambda}(t)) \geq 0, \\ 0 & \text{otherwise.} \end{cases} \quad (64)$$

Control law T for the altitude subsystem is chosen as

$$T = \frac{1}{\hat{\lambda} c\phi c\theta} (e_z + e_w \kappa_w + g - \ddot{z}_d + \kappa_z \dot{e}_z). \quad (65)$$

so that $\dot{V}_{QM_w} = -\kappa_z e_z^2 - \kappa_w e_w^2$ which guarantees asymptotic stable system for appropriately chosen $\kappa_z, \kappa_w > 0$.

By using the adaptive law (64), the control laws for roll, pitch, yaw, u_x and u_y defined by using the same procedure are

$$\begin{aligned} L_r = & \left(\frac{b_y}{b_3 b_y - b_4} \right) (-e_\phi - \kappa_p e_p - \kappa_\phi \dot{e}_\phi + \ddot{\phi}_d - b_1 r q - b_2 p q \\ & - \frac{b_4}{b_y} (-e_\psi - \kappa_r e_r - \kappa_\psi \dot{e}_\psi + \ddot{\psi}_d - b_8 p q + b_2 q r)) - L_a, \end{aligned} \quad (66)$$

$$M_t = \frac{1}{b_7} (\ddot{\theta}_d - e_\theta - \kappa_q e_q - \kappa_\theta \dot{e}_\theta + b_6 (p^2 - r^2) - b_5 p r), \quad (67)$$

$$N_t = \frac{1}{b_9} (\ddot{\psi}_d - e_\psi - \kappa_r e_r - \kappa_\psi \dot{e}_\psi - (b_8 p - b_2 r) q - b_4 L_t), \quad (68)$$

$$u_x = \frac{1}{T\hat{\lambda}} (e_x + \kappa_u e_u - \ddot{x}_d + \kappa_x \dot{e}_x), \quad (69)$$

$$u_y = \frac{1}{T\hat{\lambda}} (e_y + \kappa_v e_v - \ddot{y}_d + \kappa_y \dot{e}_y). \quad (70)$$

5 | CONTROL ALLOCATION

A drone propulsion system consists of a speed controller, DC motor, and propellers designed for maximum efficiency in the entire available speed range [55]. A variable pitch propulsion system-based drone with constant rotor speed uses a single power plant by varying the combined pitch angle of the blades for thrust actuation. Such a mechanism provides advantages like (i) thrust in both upward and downward directions utilizing positive and negative pitch, (ii) reduced power consumption by optimizing pitch and rotational speed, and (iii) modified rotational speed for maximal thrust. Figure 7 shows the Block diagram of a variable pitch propulsion system such that the pitch of the rotor gets adjusted by the servo system connected to a ball-bearing joint for desired moments.

Momentum theory and Blade Element Theory (BET) help find the torque and thrust generated as thrust coefficient functions. The mathematical expression of blade pitch angle for rotor i is

$$\theta_{0_i} = \frac{6CT_i}{\sigma C_{l_\alpha}} + \frac{3}{2} \sqrt{\frac{CT_i}{2}}, \quad (71)$$

where T_i is the thrust generated by the rotor i , $CT_i = \frac{T_i}{\rho \pi R^2 V_{tip}^2}$

is the thrust coefficient, $\sigma = \frac{cN_b}{\pi R}$ is solidity ratio, C_{l_α} is the lift curve's slope, ρ is air density, $V_{tip} = \omega R$ is the angular velocity of the blade tip, R is the rotor's radius, N_b is number of blades at each rotor, and c is the chord length and α_b is Angle of Attack (AoA) of blade.

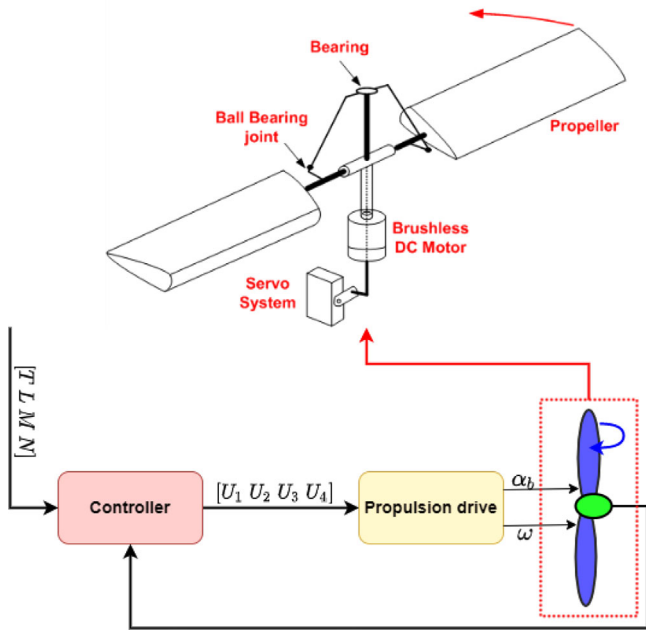


FIGURE 7 Variable pitch propulsion system for biplane

To control roll, pitch and yaw movements and altitude while in quadrotor mode or fixed-wing mode, the desired input from the control law is defined in (15) - (18) and in fixed-wing mode (47), (37), (58), and (59). The total thrust and moments for variable pitch propeller system [56] is given as

$$\begin{bmatrix} T \\ L_t \\ M_t \\ N_t \end{bmatrix} = \begin{bmatrix} k & k & k & k \\ k \cdot d & -k \cdot d & -k \cdot d & k \cdot d \\ k \cdot d & k \cdot d & -k \cdot d & -k \cdot d \\ C_1 & -C_2 & C_3 & -C_4 \end{bmatrix} \begin{bmatrix} CT_1 \\ CT_2 \\ CT_3 \\ CT_4 \end{bmatrix}, \quad (72)$$

where $k = \rho \pi R^2 V_{tip}$, $V_{tip} = \Omega \cdot R$, $\Omega = 3200$ for hovering mode and $\Omega = 2000$ for fixed-wing mode [45], $C_i = \frac{k \cdot R}{\sqrt{2}} (|CT_i|)^{1/2}$, $i = 1, \dots, 4$. In the first iteration, we calculate the thrust coefficient by taking inverse of (72), given as

$$\begin{bmatrix} CT_1 \\ CT_2 \\ CT_3 \\ CT_4 \end{bmatrix} = \begin{bmatrix} k & k & k & k \\ k \cdot d & -k \cdot d & -k \cdot d & k \cdot d \\ k \cdot d & k \cdot d & -k \cdot d & -k \cdot d \\ C_1 & -C_2 & C_3 & -C_4 \end{bmatrix}^{-1} \begin{bmatrix} T \\ L_t \\ M_t \\ N_t \end{bmatrix}. \quad (73)$$

By using these thrust coefficients, the desired input for quadrotor biplane are calculated for subsequent iterations to find $U_1 = T$, $U_2 = L_t$, $U_3 = M_t$, and $U_4 = N_t$ as given in (72).

6 | RESULTS AND DISCUSSIONS

Simulation is carried out by using parameters [46] given in Table 1.

TABLE 1 Simulation parameters

Parameters	Value
g	9.8 m/s ²
Mass (m)	12 kg
I_{xx}	1.86 kg · m ²
I_{yy}	2.03 kg · m ²
I_{zz}	3.617 kg · m ²
Wing area (single)	0.754 m ²
Aspect ratio	6.9
Wing Span	2.29 m
Gap-to-chord ratio	2.56

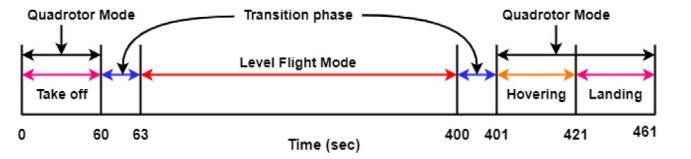


FIGURE 8 Simulation time line for trajectory tracking

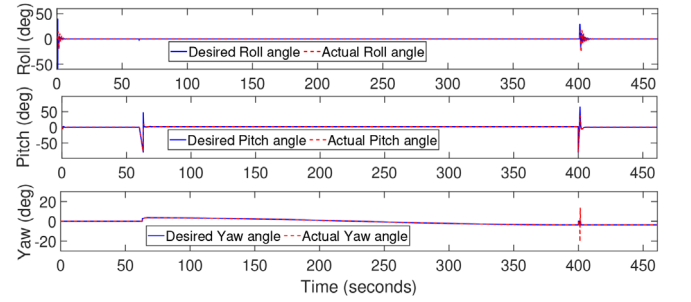


FIGURE 9 Attitude during trajectory tracking

6.1 | Trajectory tracking

Figure 8 provides the Simulation timeline for trajectory tracking. For $t = 0 - 40$ s, the biplane is commanded to take-off with constant velocity of 5 m/s and in hovering state till $t = 60$ after reaching 200 m altitude. Then it performs transition maneuver in next 3 s to reach $\approx 90^\circ$ pitch angle, and then effectively converts to a fixed-wing UAV to fly at 15 m/s in $t = 63 - 400$ s. It is then commanded to transition in 1 s and then be in hover state for the next 20 s. At $t = 421$ s, the landing phase is initiated with 5 m/s constant velocity to land at $t = 461$. There is no change in mass during the whole flight envelope, and the backstepping controller ensures trajectory tracking. The associated simulation results are given next.

Figure 9 shows the attitude in trajectory tracking with the backstepping controller to effectively track all desired angles in all modes. However, there are fluctuations for a short duration in attitude while switching the quadrotor to level flight and back to the quadrotor mode. Figure 10 shows the backstepping controller's good position tracking performance. A 2 m error gets generated in altitude while changing the quadrotor to level and

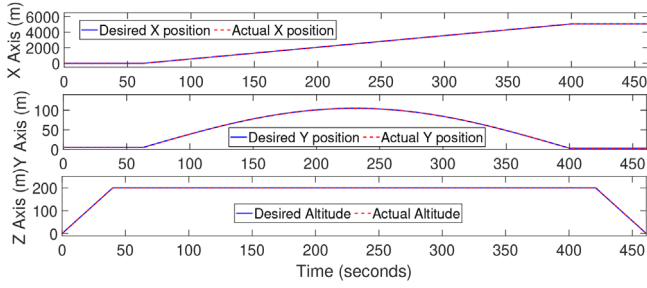


FIGURE 10 Position during trajectory tracking

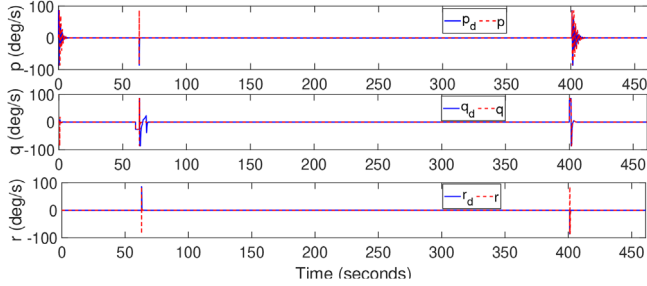


FIGURE 11 Angular velocity during trajectory tracking

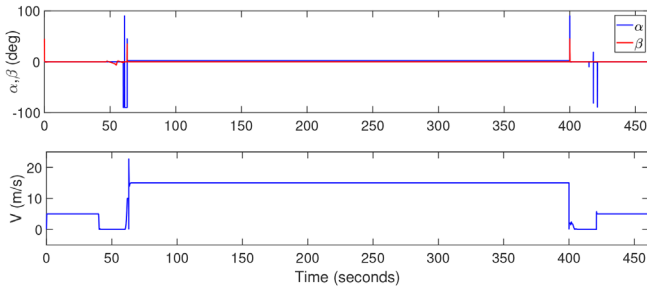


FIGURE 12 AOA, slide slip angle and vehicle velocity

vice versa. There is a 6m error in the x axis while transitioning to quadrotor and then to level flight mode, and 0.5m error in the y axis because there is no control over the $x - y$ positions during transition.

Figure 11 shows the angular velocity tracking of the biplane during the entire flight envelope. Figure 12 provides the angle of attack (α), slide slip angle (β), and total velocity of the vehicle during the entire regime of trajectory tracking. During level flight AoA (α) is around 3° and the slide slip angle is at zero deg. The velocity of the biplane is 15 m/s during flight mode and 5 m/s during take-off and landing. Figure 13 shows the thrust coefficients during the flight, and Figure 14 depicts the thrust and moments. The generated thrust is significantly lower than the thrust needed in the quadrotor mode.

Figure 15 describes a three-dimensional trajectory tracking showing that the proposed backstepping controller efficiently tracks the desired path, barring minor fluctuations during the transition from fixed-wing to quadrotor mode and vice versa.

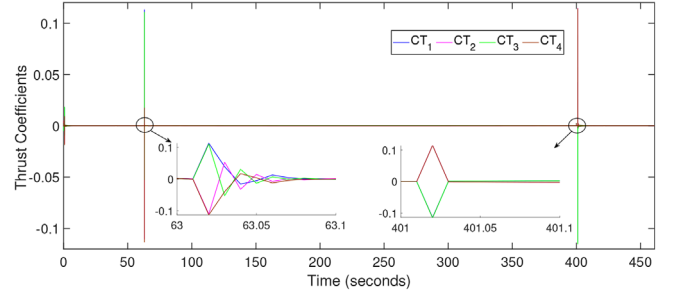


FIGURE 13 Thrust coefficient during trajectory tracking

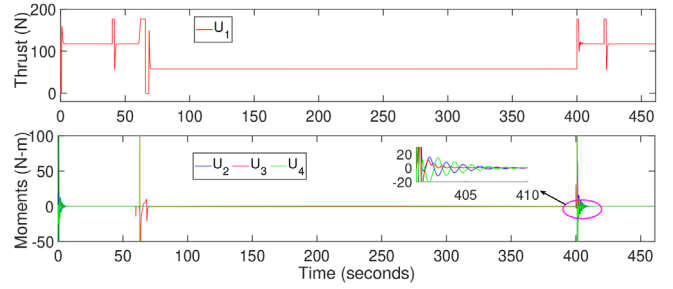


FIGURE 14 Control signals during trajectory tracking

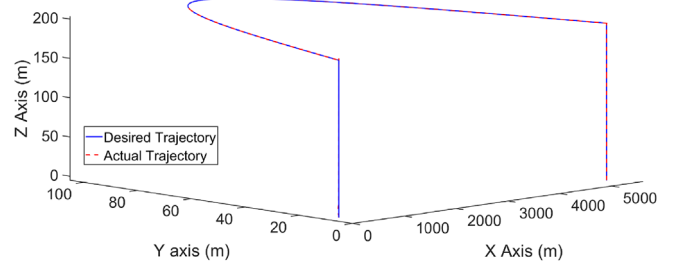


FIGURE 15 3-D trajectory tracking

6.2 | Packet delivery scenario simulation

Atmospheric turbulence is of significant importance in the assessment of aircraft performance and in calculating structural loads and aircraft handling qualities [57]. So for this simulation study, we apply the wind gust turbulence model to the entire flight regime to create a real-time scenario for packet delivery. Figure 16 shows the graphical representation timeline of the simulation. With a net weight of 18 kg in the beginning, the biplane quadrotor takes-off at $[0.5 \ 5 \ 0]$ location with 1 m/s velocity up to $t = 20$ s. At 20 m height, it is commanded to perform transition maneuver till $t = 23$ s, and then flies in level flight mode till $t = 100$ s to again perform transition to change to quadrotor mode for payload drop at $t = 105$ s, to again perform transition maneuver during $t = 110$ to $t = 113$ s, and fly to the next location for 3 kg payload by dropping the altitude from 20 m to 2 m. At $t = 193$ s and $t = 287$ s biplane picks up a payload of 3 kg each. At $t = 299$ s, wind gust is applied to create a more realistic scenario when coming back to the origin at $t = 517$ s and commanded to land for next 20 s.

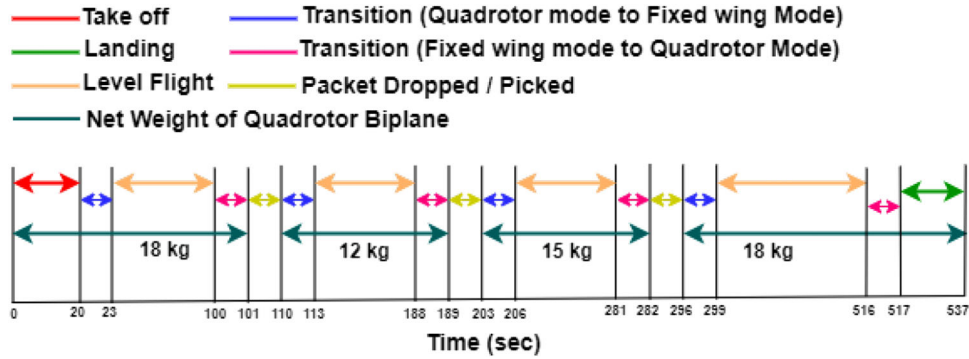


FIGURE 16 Simulation timeline for Packet delivery

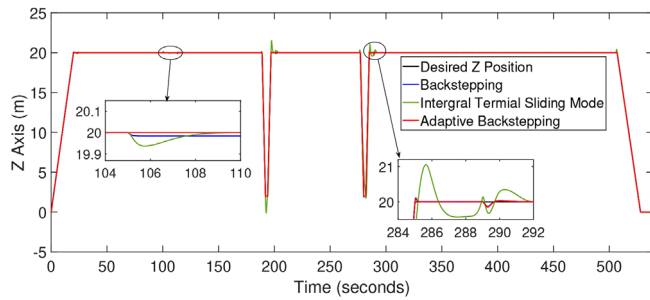


FIGURE 17 Altitude during packet delivery

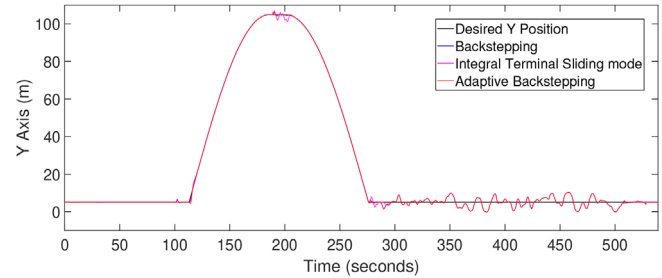


FIGURE 19 Y position during packet delivery

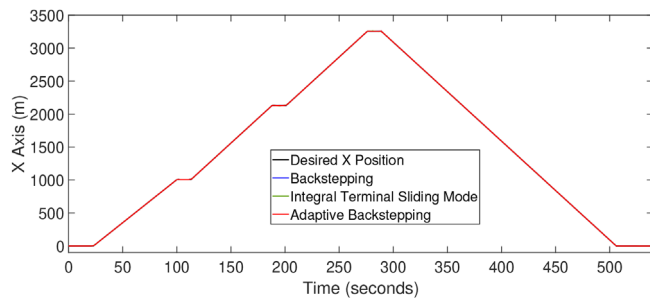


FIGURE 18 X position during packet delivery

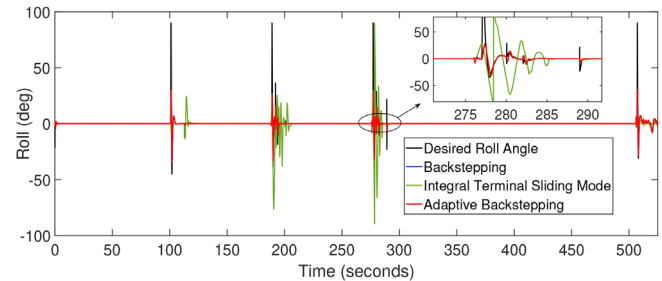


FIGURE 20 Roll angle during packet delivery

Figure 17 shows the altitude tracking by backstepping, ITSMC, and adaptive backstepping controller during payload delivery. After a drop of 6 kg payload, an 8 cm error is generated in altitude in the case of the backstepping controller, while there is no steady-state error in the case of the ITSMC controller but takes 4 s to track the desired altitude again, making ITSMC comparatively slower than backstepping method. The adaptive backstepping controller adapts to the changes and effectively tracks altitude. Compared to the ITSMC, the adaptive backstepping controller is fast to reach the desired altitude in transition maneuver, as observable in $t = 284 - 292$ s. While applying wind gust at $t = 299$ s, there is no significant change in altitude. Figure 18 shows efficient tracking of x axis trajectory through backstepping, ITSMC and adaptive backstepping controller, with no significant impact of wind gusts. There is a small error when mass changes during $t = 23$ to $t = 100$, $t = 113$ to $t = 188$,

$t = 206$ to $t = 281$ and $t = 299$ to $t = 2517$ s. The velocity in x direction is 15 m/s. There are fluctuations in the y axis trajectory (Figure 19) because of wind gusts, with no significant change during mass change but there is error generated by backstepping and ITSMC during the transition between quadrotor to fixed-wing and vice versa.

Figure 20 shows roll angle tracking during payload delivery. There is a sudden change after the transition from quadrotor mode to level flight mode. Backstepping, ITSMC, and adaptive backstepping controllers efficiently track the desired roll angle, but ITSMC has a more sluggish response. There is no significant fluctuation in the roll angle during wind gusts in the level flight mode but in quadrotor mode while landing. Figure 21 shows the pitch angle tracking during payload delivery. In the quadrotor mode, the pitch angle is around 0° . The transition mode commands the pitch angle to rotate $\approx -90^\circ$ to transition from the quadrotor mode into the fixed-wing mode and back to the

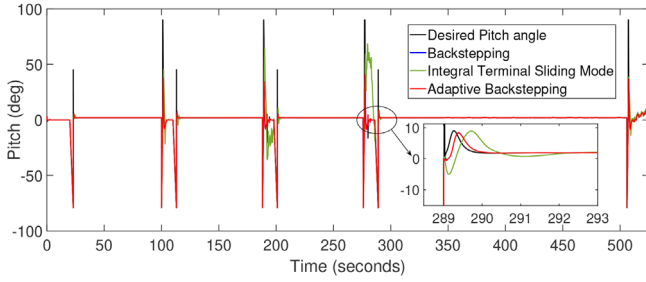


FIGURE 21 Pitch angle during packet delivery

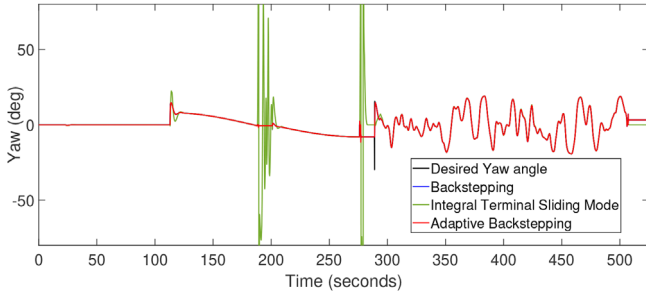


FIGURE 22 Yaw angle during packet delivery

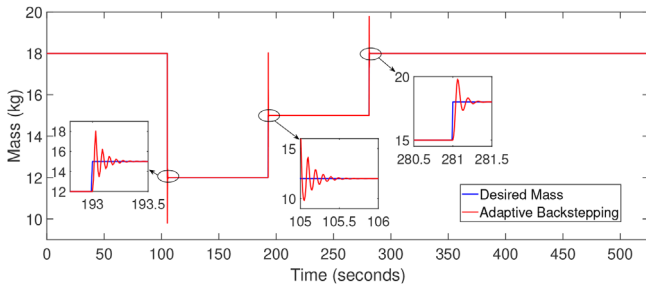


FIGURE 23 Mass tracking by the designed adaptive law

quadrotor mode by rotating about $\approx +90^\circ$. The adaptive backstepping controller performs better in these transitions than the backstepping and ITSMC controller. Wind gusts cause noticeable fluctuations in the pitch angle while landing.

Figure 22 shows yaw angle tracking during the entire flight envelope by backstepping, ITSMC, and adaptive backstepping controllers. ITSMC controller encounters a short duration spike in the yaw angle during state change, but backstepping and adaptive backstepping controllers see relatively lesser variations. There is a fluctuation due to the wind gust in fixed-wing mode, and backstepping, ITSMC, and adaptive backstepping are equally effective in tracking the desired yaw angle. Figure 23 shows the response of adaptive law while mass change happens in the biplane quadrotor. Any change in mass gets tracked by the adaptive law within 1 s during both pick-up and drop.

Figure 24 shows the trust profile during the whole flight envelope. For example, at $t = 105$ s, the generated thrust is 177 N. After a drop of 6 kg, the thrust is 117 N. This significant change in thrust is due to the mass change. There are fluctua-

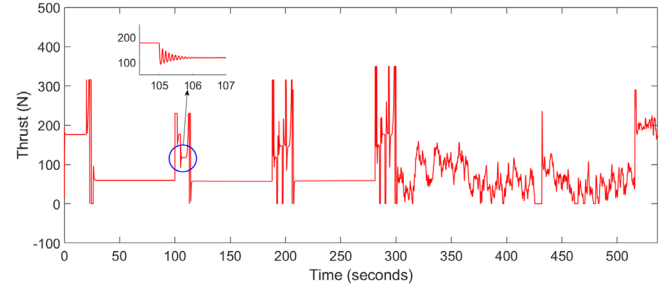


FIGURE 24 Change in trust during mass change

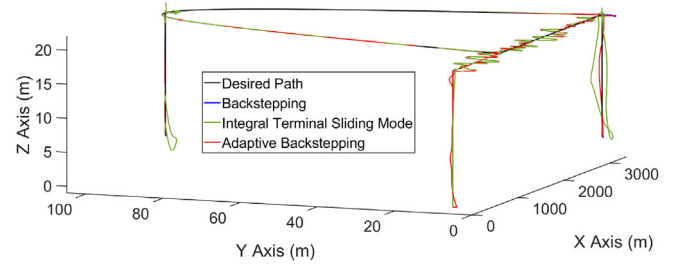


FIGURE 25 3-D trajectory tracking

tions in thrust to compensate for the effect of wind gusts on the biplane quadrotor.

Figure 25 shows a three-dimensional trajectory tracking mission and the effect of variation in mass and wind gusts by applying backstepping, ITSMC and adaptive backstepping control methods.

7 | CONCLUSIONS

Hybrid vehicles like biplanes have advantages of both fixed-wing and rotary-wing. In this simulation study, we evaluate a backstepping controller's performance for trajectory tracking, consisting of take-off, hovering, transition, level flight, and landing phases, and find minimal errors in position and angle tracking. For example, the $x - y$ position error in the transition phase is because there is no control over the $x - y$ axis, only over the altitude and attitude in transition. In the second phase of the simulation study, we compare the responses with a backstepping controller, ITSMC, and adaptive backstepping for payload delivery. Wind gust is applied to create a more realistic scenario between $t = 299 - 537$ s. Results show a 10 cm steady-state error in altitude generated by the backstepping. At the same time, ITSMC can track the desired altitude but takes 4 s to track the altitude, and adaptive backstepping easily adapts to mass change at $t = 105$ s from 18 kg to 12 kg. After the transition, ITSMC takes more time than backstepping and adaptive backstepping controllers to reach the desired states. We need precise altitude tracking to pick up the payloads in the hovering state. Simulation results also show a small error generated in the $x - y$ axis when mass changes, but in the presence of the wind gust, the position error generated by all three controllers is not negligible in the y axis. The adaptive backstepping controller

efficiently tracks the attitude of the biplane during payload delivery, and there is a concise time error generated while changing the mode. Yaw angle oscillates during level flight mode due to the wind gust, and the effect is more in pitch and roll angles with the biplane in quadrotor mode. The overall outcomes are

- For trajectory tracking, the backstepping controller effectively tracks the biplane's position and attitude in all modes and phases.
- For payload delivery, adaptive backstepping performs better than the backstepping and ITSMC controllers.
- Yaw angle oscillates in level flight mode while pitch and roll angles fluctuate in quadrotor mode in the presence of wind gusts.
- The Backstepping controller generates a steady-state error with mass changes while ITSMC takes time to get the desired altitude again. In contrast, the adaptive law for an altered parameter in an adaptive backstepping controller gives zero steady-state error and faster response than the ITSMC.

After successfully implementing the proposed control scheme in Matlab Simulink, the next task is to use ROS (robot operating system) and Simulink to simulate the design in Gazebo, an open-source 3D robotics simulator. This step is expected to give us more information about the behavior of the biplane quadrotor during the mission and the performance of the observer-based backstepping controller. And finally, using the PX4 flight controller and Simulink, we will apply this control method on the actual biplane quadrotor.

ACKNOWLEDGEMENTS

The publication of this article was funded by Qatar National Library.

CONFLICT OF INTEREST

The authors have declared no conflict of interest.

ORCID

Nibal Dalwadi  <https://orcid.org/0000-0002-9958-8259>

Dipankar Deb  <https://orcid.org/0000-0003-4419-4516>

S. M. Muryeen  <https://orcid.org/0000-0003-4955-6889>

REFERENCES

1. Hrishikeshavan, V., Bogdanowicz, C., Chopra, I.: Design, performance and testing of a quad rotor biplane micro air vehicle for multi role missions. *Int. J. Micro Air Veh.* 6(3), 155–173 (2014)
2. Sridharan, A., Govindarajan, B., Chopra, I.: A scalability study of the multi-rotor biplane tailsitter using conceptual sizing. *J. American Helicopter Soc.* 65 (2019)
3. Dawkins, J., DeVries, L.: Modeling, trim analysis, and trajectory control of a micro-quadrotor with wings. *Drones* 2(2), 21 (2018)
4. Hrishikeshavan, V., Bawek, D., Rand, O., Chopra, I.: Control of a quad rotor biplane micro air vehicle in transition from hover to forward flight. In: *American Helicopter Society Specialists Meeting on Unmanned Rotorcraft and Network Centric Operations*. AHS International Alexandria, (2013)
5. Mathew, N., Smith, S.L., Waslander, S.L.: Planning paths for package delivery in heterogeneous multirobot teams. *IEEE Trans. Autom. Sci. Eng.* 12(4), 1298–1308 (2015)
6. Liu, D., Liu, H., Lewis, F.L., Valavanis, K.P.: Robust time-varying formation control for tail-sitters in flight mode transitions. *IEEE Transactions on Systems, Man, and Cybernetics: Systems* 51(7), 4102–4111 (2021)
7. Liu, H., Peng, F., Lewis, F.L., Wan, Y.: Robust tracking control for tail-sitters in flight mode transitions. *IEEE Trans. Aerosp. Electron. Syst.* 55(4), 2023–2035 (2019)
8. Wagter, C.D., Meulenbeld, J.: Modeling the unstable DelftaCopter vertical take-off and landing tailsitter unmanned air vehicle in hover and forward flight from flight test data. *Int. J. Micro Air Veh.* 11, 175682931988030 (2019)
9. Mofid, O., Mobayen, S., Wong, W.K.: Adaptive terminal sliding mode control for attitude and position tracking control of quadrotor uavs in the existence of external disturbance. *IEEE Access* 9, 3428–3440 (2021)
10. Kumar Muthusamy, P., Garratt, M., Pota, H.R., Muthusamy, R.: Realtime adaptive intelligent control system for quadcopter uav with payload uncertainties. *IEEE Trans. Ind. Electron.* (2021)
11. Sartori, D., Quagliotti, F., Rutherford, M.J., Valavanis, K.P.: Design and development of a backstepping controller autopilot for fixed-wing UAVs. *The Aeronautical Journal* 125(1294), 2087–2113 (2021)
12. Chen, F., Jiang, R., Zhang, K., Jiang, B., Tao, G.: Robust backstepping sliding-mode control and observer-based fault estimation for a quadrotor uav. *IEEE Trans. Ind. Electron.* 63(8), 5044–5056 (2016)
13. Luo, C., Du, Z., Yu, L.: Neural network control design for an unmanned aerial vehicle with a suspended payload. *Electronics* 8(9), 931 (2019)
14. Dalwadi, N., Deb, D., Kothari, M., Ozana, S.: Disturbance observer-based backstepping control of tail-sitter UAVs. *Actuators* 10(6), 119 (2021)
15. Lungu, M.: Backstepping and dynamic inversion combined controller for auto-landing of fixed wing UAVs. *Aerosp. Sci. Technol.* 96, 105526 (2020)
16. He, W., Wang, T., He, X., Yang, L.J., Kaynak, O.: Dynamical modeling and boundary vibration control of a rigid-flexible wing system. *IEEE/ASME Trans. Mechatron.* 25(6), 2711–2721 (2020)
17. He, W., Mu, X., Zhang, L., Zou, Y.: Modeling and trajectory tracking control for flapping-wing micro aerial vehicles. *IEEE/CAA J. Autom. Sin.* 8(1), 148–156 (2021)
18. Yang, T., Sun, N., Chen, H., Fang, Y.: Neural network-based adaptive anti-swing control of an underactuated ship-mounted crane with roll motions and input dead zones. *IEEE Trans. Neural Networks Learn. Syst.* 31(3), 901–914 (2020)
19. Deb, D., Burkholder, J., Tao, G.: Signal-dependent uncertainty compensation: A general framework. In: *Adaptive Compensation of Nonlinear Actuators for Flight Control Applications*, pp. 83–98. Springer, Singapore (2021). https://doi.org/10.1007/978-981-16-4161-9_5
20. Deb, D., Burkholder, J., Tao, G.: NN-based high-order adaptive compensation framework for signal dependencies. In: *Adaptive Compensation of Nonlinear Actuators for Flight Control Applications*, pp. 99–111. Springer, Singapore (2021). https://doi.org/10.1007/978-981-16-4161-9_6
21. Yang, T., Sun, N., Fang, Y.: Adaptive fuzzy control for a class of mimo underactuated systems with plant uncertainties and actuator deadzones: Design and experiments. *IEEE Trans. Cybern.* 1–14 (2021)
22. Wang, H., Kang, S., Zhao, X., Xu, N., Li, T.: Command filter-based adaptive neural control design for nonstrict-feedback nonlinear systems with multiple actuator constraints. *IEEE Trans. Cybern.* 1–10 (2021)
23. Lei, W., Li, C., Chen, M.Z.Q.: Robust adaptive tracking control for quadrotors by combining pi and self-tuning regulator. *IEEE Trans. Control Syst. Technol.* 27(6), 2663–2671 (2019)
24. Dydek, Z.T., Annaswamy, A.M., Lavretsky, E.: Adaptive control of quadrotor uavs: A design trade study with flight evaluations. *IEEE Trans. Control Syst. Technol.* 21(4), 1400–1406 (2013)
25. Zuo, Z., Mallikarjunan, S.: \mathcal{L}_1 adaptive backstepping for robust trajectory tracking of uavs. *IEEE Trans. Ind. Electron.* 64(4), 2944–2954 (2017)
26. Mofid, O., Mobayen, S., Fekih, A.: Adaptive integral-type terminal sliding mode control for unmanned aerial vehicle under model uncertainties and external disturbances. *IEEE Access* 9, 53255–53265 (2021)
27. Mofid, O., Mobayen, S., Zhang, C., Esakki, B.: Desired tracking of delayed quadrotor UAV under model uncertainty and wind disturbance using adaptive super-twisting terminal sliding mode control. *ISA Trans.* (2021)

28. Mofid, O., Mobayen, S.: Adaptive finite-time back-stepping global sliding mode tracker of quad-rotor uavs under model uncertainty, wind perturbation and input saturation. *IEEE Trans. Aerosp. Electron. Syst.* (2021)
29. Kourani, A., Daher, N.: Leveraging pid gain selection towards adaptive backstepping control for a class of second-order systems. In: 2021 American Control Conference (ACC), pp. 1174–1179. IEEE, Piscataway (2021)
30. Dhaybi, M., Daher, N.: Accurate real-time estimation of the inertia tensor of package delivery quadrotors. In: 2020 American Control Conference (ACC). IEEE, Piscataway (2020)
31. Navabi, M., Davoodi, A., Mirzaei, H.: Trajectory tracking of under-actuated quadcopter using lyapunov-based optimum adaptive controller. *Proc. Inst. Mech. Eng., Part G: J Aerospace Engineering* 0954410021110108 (2021)
32. Hsu, C.F., Lin, C.M., Lee, T.T.: Wavelet adaptive backstepping control for a class of nonlinear systems. *IEEE Trans. Neural Networks* 17(5), 1175–1183 (2006)
33. Sun, W., Gao, H., Kaynak, O.: Adaptive backstepping control for active suspension systems with hard constraints. *IEEE/ASME Trans. Mechatron.* 18(3), 1072–1079 (2013)
34. Liu, D., Liu, H., Zhang, J., Lewis, F.L.: Adaptive attitude controller design for tail-sitter unmanned aerial vehicles. *J. Vib. Control* 27(1-2), 185–196 (2020)
35. Wang, H., Xu, K., Qiu, J.: Event-triggered adaptive fuzzy fixed-time tracking control for a class of nonstrict-feedback nonlinear systems. *IEEE Trans. Circuits Syst. I Regul. Pap.* (2021)
36. Oshman, Y., Isakow, M.: Mini-uav altitude estimation using an inertially stabilized payload. *IEEE Trans. Aerosp. Electron. Syst.* 35(4), 1191–1203 (1999)
37. Qian, L., Liu, H.H.: Path-following control of a quadrotor uav with a cable-suspended payload under wind disturbances. *IEEE Trans. Ind. Electron.* 67(3), 2021–2029 (2020)
38. Yang, S., Xian, B.: Energy-based nonlinear adaptive control design for the quadrotor uav system with a suspended payload. *IEEE Trans. Ind. Electron.* 67(3), 2054–2064 (2020)
39. Lee, S., Son, H.: Antisway control of a multirotor with cable-suspended payload. *IEEE Trans. Control Syst. Technol.* 1–9 (2020)
40. Xian, B., Wang, S., Yang, S.: An online trajectory planning approach for a quadrotor uav with a slung payload. *IEEE Trans. Ind. Electron.* 67(8), 6669–6678 (2020)
41. Outeiro, P., Cardeira, C., Oliveira, P.: Multiple-model control architecture for a quadrotor with constant unknown mass and inertia. *Mechatronics* 73, 102455 (2021)
42. Qian, L., Graham, S., Liu, H.H.: Guidance and control law design for a slung payload in autonomous landing: A drone delivery case study. *IEEE/ASME Trans. Mechatron.* 25(4), 1773–1782 (2020)
43. Phillips, P., Hrishikeshavan, V., Rand, O., Chopra, I.: Design and development of a scaled quadrotor biplane with variable pitch propellers for rapid payload delivery. *Proceedings of the American Helicopter Society 72nd Annual Forum*, pp. 17–19. West Palm Beach FL, USA (2016)
44. Phillips, B., Hrishikeshavan, V., Yeo, D., Chopra, I., Rand, O.: Flight performance of a package delivery quadrotor biplane. In: 7th AHS Technical Meeting on VTOL Unmanned Aircraft Systems, PP. 1–11. IEEE, (2017)
45. Chipade, V.S., Kothari, M., Chaudhari, R.R., et al.: Systematic design methodology for development and flight testing of a variable pitch quadrotor biplane vtol uav for payload delivery. *Mechatronics* 55, 94–114 (2018)
46. Swarnkar, S., Parwana, H., Kothari, M., Abhishek, A.: Biplane-quadrotor tail-sitter uav: Flight dynamics and control. *Journal of Guidance, Control, and Dynamics* 41(5), 1049–1067 (2018)
47. Govindarajan, B., Sridharan, A.: Conceptual sizing of vertical lift package delivery platforms. *Journal of Aircraft* 57(6), 1170–1188 (2020)
48. Morgado, J., Vizinho, R., Silvestre, M.A.R., Páscoa, J.C.: XFOIL vs CFD performance predictions for high lift low Reynolds number airfoils. *Aerosp. Sci. Technol.* 52, 207–214 (2016)
49. Lafountain, C., Cohen, K., Abdallah, S.: Use of XFOIL in design of camber-controlled morphing UAVs. *Comp. Appl. Eng. Education* 20(4), 673–680 (2010)
50. Basri, M.A.M., Husain, A.R., Danapalasingam, K.A.: Enhanced backstepping controller design with application to autonomous quadrotor unmanned aerial vehicle. *J. Intell. Rob. Syst.* 79(2), 295–321 (2014)
51. Deb, D., Tao, G., Burkholder, J.O.: An adaptive inverse compensation scheme for signal-dependent actuator nonlinearities. In: 2007 46th IEEE Conference on Decision and Control. IEEE, Piscataway (2007)
52. Deb, D., Tao, G., Burkholder, J.O., Smith, D.R.: Adaptive synthetic jet actuator compensation for a nonlinear tailless aircraft model at low angles of attack. In: 2006 American Control Conference. IEEE, Piscataway (2006)
53. Kapoor, D., Deb, D., Sahai, A., Bangar, H.: Adaptive failure compensation for coaxial rotor helicopter under propeller failure. In: 2012 American Control Conference (ACC). IEEE, Piscataway (2012)
54. Ambati, P.R., Padhi, R.: A neuro-adaptive augmented dynamic inversion design for robust auto-landing. *IFAC Proc.* 47(3), 12202–12207 (2014)
55. Gebauer, J., Wagnerová, R., Smutný, P., Podešva, P.: Controller design for variable pitch propeller propulsion drive. *IFAC-PapersOnLine* 52(27), 186–191 (2019)
56. Gupta, N., Kothari, M., Abhishek: Modeling and control of inverted flight of a variable-pitch quadrotor. *CoRR*, abs/1709.06407 (2017). Available from: <http://arxiv.org/abs/1709.06407>
57. Beal, T.R.: Digital simulation of atmospheric turbulence for dryden and von karman models. *J. Guidance Control Dynamics* 16(1), 132–138 (1993)

How to cite this article: Dalwadi, N., Deb, D., Muyeen, S.M.: Adaptive backstepping controller design of quadrotor biplane for payload delivery. *IET Intell. Transp. Syst.* 1–15 (2022).
<https://doi.org/10.1049/itr2.12171>